Northward shift of the southern westerlies during the Antarctic Cold Reversal

Fletcher, M.-S., Pedro, J., Hall, T., Mariani, M., Alexander, J. A., Beck, K., Blaauw, M., Hodgson, D., Heijnis, H., Gadd, P., & Lisé-Pronovost, A. (2021). Northward shift of the southern westerlies during the Antarctic Cold Reversal. *Quaternary Science Reviews*, *271*, Article 107189. https://doi.org/10.1016/j.quascirev.2021.107189

Highlights:

We present empirical palaeoclimate data that demonstrate a northward shift of the southern westerly wind during the Antarctic Cold Reversal (ACR) that drove antiphase west-east environmental responses across the island of Tasmania.

Stronger westerly wind flow over Tasmania during the ACR drove wetter conditions on the western (windward) slopes of the Tasmanian mountains that dampened regional fire activity and drove regional vegetation change toward more cold tolerant plant communities.

Stronger westerly wind flow over Tasmania during the ACR drove increased evaporation on the eastern (leeward) side of the Tasmanian mountains.

Our results support that millennial scale climate variability involves global reorganisation of ocean and atmospheric circulation and heat transport.

Graphical Abstract for Northward shift of the southern westerlies during the Antarctic Cold Reversal

Fletcher, Michael-Shawn[1,2*], Pedro, Joel[3, 4], Hall, Tegan[1], Mariani, Michela[1,5], Alexander, Joseph A.[1], Beck, Kristen[1,6], Blaauw, Maarten[7], Hodgson, Dominic A.[8], Heijnis, Henk[9], Gadd, Patricia. S.[9], Lise-Pronovost, Agathe[10]

Correspondence to: michael.fletcher@unimelb.edu.au

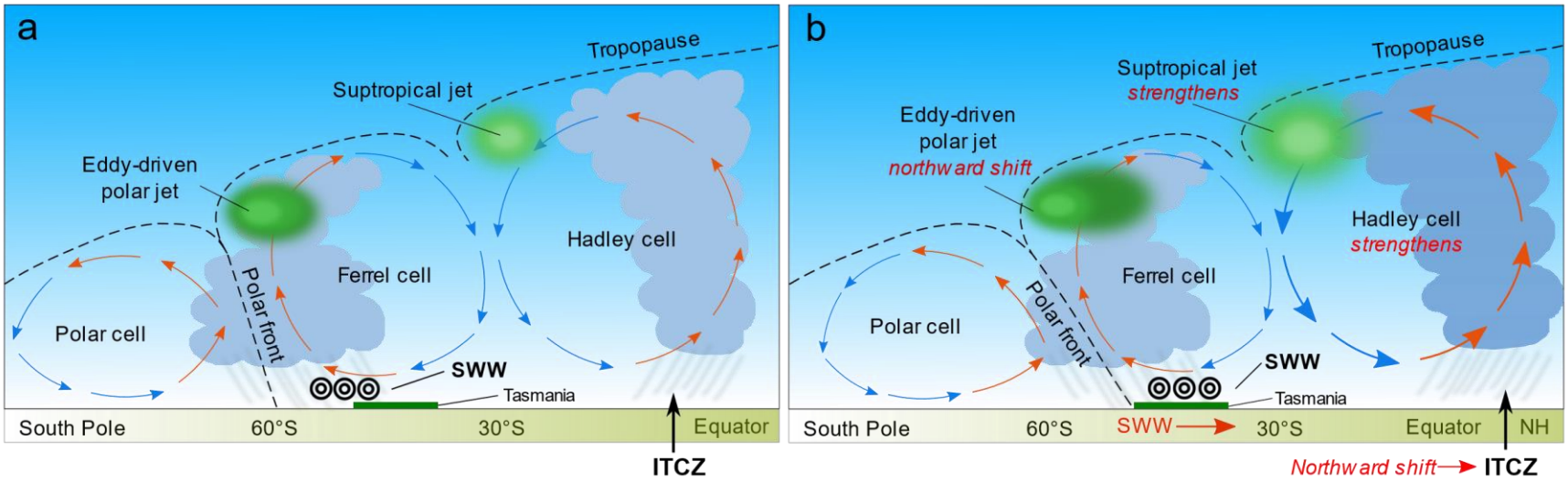

Figure. S6.
Schematic illustrating (a) the approximate latitudinal positions of major components of Southern Hemisphere atmospheric system pre-northward shift of the ITCZ, and (b) atmospheric processes involved in the northward shift of the ITCZ and southern westerlies (SWW). Schematic shows a northward intensification of the Southern Hemisphere winter Hadley circulation, which delivers increased heat and eddy-momentum flux into the Southern Hemisphere subtropics. The increased momentum flux strengthens the subtropical jet and pulls the eddy driven polar jet (of which the surface expression is the southern westerlies) northward.

Article Type: Short Communication

Northward shift of the southern westerlies during the Antarctic Cold Reversal

Authors: Fletcher, Michael-Shawn[1,2*], Pedro, Joel[3, 4], Hall, Tegan[1], Mariani, Michela[1,5], Alexander, Joseph A.[1], Beck, Kristen[1,6], Blaauw, Maarten[7], Hodgson, Dominic A.[8], Heijnis, Henk[9], Gadd, Patricia. S.[9], Lise-Pronovost, Agathe[1]

Affiliations:

[1]School of Geography, Earth and Atmospheric Sciences, University of Melbourne, Victoria, Australia

[2]Indigenous Knowledge Institute, University of Melbourne, Victoria, Australia

[3]Australian Antarctic Division (AAD), Kingston, Tasmania, Australia

[4]Australian Antarctic Program Partnership, Institute for Marine and Antarctic Studies, University of Tasmania, Hobart, Tasmania

[5]School of Geography, University of Nottingham, Nottingham, United Kingdom

[6]Lincoln Centre for Water and Planetary Health, School of Geography, University of Lincoln, Lincoln, United Kingdom

[7]School of Natural and Built Environment, Queen's University Belfast, United Kingdom

[8]British Antarctic Survey, Cambridge & Department of Geography, Durham University, United Kingdom

[9]Australian Nuclear Science and Technology Organisation, New South Wales, Australia

*Corresponding author: michael.fletcher@unimelb.edu.au

Abstract: Inter-hemispheric asynchrony of climate change through the last deglaciation has been theoretically linked to latitudinal shifts in the southern westerlies via their influence over CO_2 out-

gassing from the Southern Ocean. Proxy-based reconstructions disagree on the behaviour of the westerlies through this interval. The last deglaciation was interrupted in the Southern Hemisphere by the Antarctic Cold Reversal (ACR; 14.7 to 13.0 ka BP (thousand years Before Present)), a millennial-scale cooling event that coincided with the Bølling–Allerød warm phase in the North Atlantic (BA; 14.7 to 12.7 ka BP). We present terrestrial proxy palaeoclimate data that demonstrate a migration of the westerlies during the last deglaciation. We support the hypothesis that wind-driven out-gassing of old CO_2 from the Southern Ocean drove the deglacial rise in atmospheric CO_2.

1.0 Introduction

The southern westerlies are part of a zonally-symmetric system that dominates the climate of the mid- to high-latitudes of the Southern Hemisphere (Garreaud, 2007). Changes in the strength and latitudinal position of the southern westerlies are believed to modulate global atmospheric CO_2 concentration via changes in wind stress over the Southern Ocean. Wind stress influences the upwelling of CO_2 saturated deep waters and the capacity of the surface ocean to absorb, or release, CO_2 (Siani et al., 2013). In the ocean, the latitudinal position of the southern westerlies is linked to the position of the Subpolar Oceanic Front and the Antarctic Circumpolar Current (Toggweiler et al., 2006), while on land changes in the southern westerlies govern mid- to high-latitude terrestrial climate, principally hydroclimate (Garreaud, 2007), which has a profound influence over a range of terrestrial processes (Fletcher and Moreno, 2012; Mariani and Fletcher, 2017). Parallel latitudinal shifts of the southern westerlies and Intertropical Convergence Zone (ITCZ) have also been proposed for the last deglaciation as part of the atmospheric response to changes in ocean heat transport by the Atlantic Meridional Overturning Circulation (AMOC) (Buizert et al., 2018; Denton et al., 2010; Markle et al., 2017; Pedro et al., 2016; Sigman et al., 2020). However, while paleoclimate proxy data confirm a cooling in the mid- to high latitudes of the Southern Hemisphere (poleward of ca. 40^{o}S) during the ACR, the available data provide no clear constraint on the latitudinal behaviour of the southern westerlies through this interval.

We reconstruct westerly wind behaviour in the mid-latitudes of the Australian sector of the Southern Hemisphere from multiproxy data from six radiocarbon-dated lake sediment sequences from Tasmania (40-44^{o}S; Figure 1a). Tasmania is uniquely situated to investigate the behaviour of the southern westerlies during the ACR due to its location at the northern margins of the westerly wind belt and an exceptionally strong correlation between southern westerly wind speed and its rainfall anomalies (Figure 1b) (Gillett et al., 2006). This means that rainfall proxies can be applied to reconstruct past changes in wind regimes. Tasmania's mountainous west coast and contrasting

lowland east coast create an orographic effect that splits the island into clear zones of positive (western sites) and negative (eastern sites) correlation between southern westerly wind speed and rainfall (Figure 1b). This allows us to target sites where there is an unambiguous southern westerly influence over rainfall.

We compile new lake sediment rainfall proxies including charcoal, pollen and geochemistry from six lakes located in zones of both significant positive and significant negative correlation between southern westerly wind speed and rainfall (Figure 1b). While the charcoal proxy is influenced by human-caused fire ignitions (Bowman and Brown, 1986), the occurrence and spread of fires is moisture-limited in the high-rainfall west of Tasmania (McWethy et al., 2013; Styger and Kirkpatrick, 2015). Sedimentary charcoal analyses have previously revealed a coherence between changes in regional charcoal (biomass burning) and changes in moisture delivery by the southern westerlies through the Holocene: increased southern westerly flow over Tasmania results in reduced sedimentary charcoal content (and vice-versa), reflecting the primacy of southern westerly-derived orographic rainfall over regional fire regimes (Mariani and Fletcher, 2017; Mariani and Fletcher, 2016).

2.0 Material and methods

2.1 Construction of age models

^{14}C analysis using accelerator mass spectrometry (AMS) was used to date each sediment record utilised in this analysis. Results for each sample submitted for analysis, along with their calibrated age ranges, are provided in Table 1. All radiocarbon ages were calibrated using SHCal20 (Hogg et al., 2020) and age-depth models for each core (Figure 3) were constructed using the *rbacon* v2.3.9.1 (Blaauw and Christen, 2011) package in R. Modelling was restricted to ~9 to 18 ka. Modelled age outputs were then used to compare regional proxy data records.

2.2 Palaeofire compilation

Palaeofire analysis was carried out using the paleofire package in R (Blarquez et al., 2014) and follows the methodology outlined in Mariani & Fletcher (2016). Three charcoal records from the precipitation-dominant western Tasmania were considered for this analysis (Lake Selina, Basin Lake and Lake Vera). Firstly, a transformation of the data was performed using the function pfTransform with MinMax, Box-Cox and Z-score methods. Transformation and standardization of different charcoal records is a highly recommended step in generating a synthesis (Blarquez et al., 2014). Here, we used the methodology proposed by Power et al. (2008) and involved a three-step data transformation including a min-max data-rescaling, variance homogenization using Box-Cox data transformation (Box and Cox, 1964), and final rescaling to Z-scores. The palaeofire composite was calculated using the function pfCompositeLF, consisting in a modified version of existing methods (Daniau et al., 2012; Marlon et al., 2008), involving a two-stage smoothing method (including LOWESS; Cleveland, 1979) of the selected bins interval. In this case, 100 years-bins were used, since it represents the best achievable resolution in order to include the majority of charcoal records for the entire reconstruction period. Confidence intervals were obtained using the function circboot with 1000 repetitions, which applies a "moving" or "circular" block bootstrap method (Kunsch, 1989) to test significance of changes in stationary time series.

2.3 Geochemical proxy analysis

Micro-X-Ray fluorescence spectrometry (µXRF) elemental profiles were obtained for three western Tasmanian records (Lake Tiberias, Lake Selina and Hazards Lagoon from the Australian Nuclear Science and Technology Organisation (ANSTO)). Cores were scanned at 0.5 mm resolution using Cox Analytical Systems ITRAX µXRF core scanner with a Mo tube (55mA current; 20s count time; 30kV voltage). Raw data were normalised to kpcs (Croudace and Rothwell, 2015). Ca/Ti ratios for each record were extracted from the full dataset as a proxy for relative evaporation levels across western Tasmania (Croudace and Rothwell, 2015).

The geochemistry of lake sediments is also influenced by changes to in-lake processes such as evaporative conditions and lake levels. The deposition of evaporative carbonate minerals into lake sediments is influenced by authigenic (within-lake) and allogenic (external catchment) processes, making it necessary to isolate the signal of authigenic deposition in order to infer changes to in-lake conditions (Cohen, 2003). For example, by normalising μXRF carbonate proxy elements (calcium and strontium) against stable detrital elements in the record, it is possible to isolate the authigenic carbonate signal (Croudace & Rothwell, 2015). This method has been widely used in paleolimnology, including in western Tasmania (Fletcher et al., 2014), and forms the basis for interpretations of in-lake conditions at Lake Rolleston. Precipitation of evaporative carbonate minerals in fresh-water lakes varies with changes to evaporative conditions and lake levels (Cohen, 2003; Haberzettl et al., 2007; Kelts and Hsü, 1978). The type of evaporative minerals that are precipitated in the water column are dependent on initial water chemistry, which is related to the underlying catchment geology (Eugster and Hardie, 1978).

2.4 Palynology

Pollen samples were prepared and analysed for the four western Tasmanian sites (Basin Lake, Lake Vera, Paddy's Lake and Lake Selina) according to standard protocols (Faegri and Iversen, 1989). Percentages of *Phyllocladus aspleniifolius* and Poaceae taxa were isolated from the full pollen datasets, focusing on the last 18 kyrs. Raw percentage data for these taxa were calculated from the terrestrial pollen sum and are presented in Figures S4 (*P. aspleniifolius*) and S5 (Poaceae). Data from all six sites were then collated into one time series to construct a regional time-series for each taxon. Prior to collation, data were standardised (transformed into z-scores) to account for differences in the mean abundances of the original datasets.

3.0 Results

All graphed results are in the Supplementary Information (Figs. S1-5) and this section only briefly describes the results here. All selected cores span the ACR interval with sufficient dating to resolve environmental changes through this interval (Figure S1). Synthesis of the charcoal records from the western Tasmanian sites (n=4) demonstrates a sharp increase in CHAR across the west commencing at ca. 17.8 ka BP and continuing until ca. 15 ka BP, before declining between ca. 13.5 ka BP. CHAR values rise again toward peak regional values at ca. 12.2 ka BP and decline thereafter (Figs 2, S3). Calculation of the Ca/Ti ratio for the evaporation-dominant sites in eastern Tasmania show a discrete peak in overall values during the ACR interval (ca. 14.7 to 13.0 ka BP) indicating a peak in calcite precipitation under evaporative conditions during this interval (Figure 2). The synthesised pollen records from the precipitation-dominant western Tasmanian sites show increased values in the hygrophilous conifer P. aspleniifolius between ca. 16-12 ka BP, with a discrete dip centred on the ACR interval (Figure S4). High Poaceae values, associated with cool temperatures in western Tasmania (Fletcher and Thomas, 2007), occur discretely during the ACR interval, embedded in a long-term decrease commencing at ca. 18 ka BP (Figure S5).

4.0 Discussion

Charcoal influx to the western Tasmanian lakes decreases during the ACR (Figs. 2d, S2-3), consistent with enhanced westerly winds and rainfall, reducing biomass burning. This change is synchronous with a marked increase in carbonate precipitation and subsequent deposition (sedimentary Ca/Ti ratio) (Kylander et al., 2011) at two sites in eastern Tasmania (Figs. 2a,b) and a concomitant decrease in carbonate deposition in the west (Figure 2c). Carbonate precipitation occurs under increased evaporative conditions in freshwater lakes (Kelts and Hsü, 1978) and the east-west anti-phasing of carbonate deposition displayed in our data during the ACR mirrors the modern rainfall-southern westerly relationship (Figure 1), suggesting an increase in wind speed over Tasmania at this time. The increasing sedimentary charcoal in the west of Tasmania immediately prior to (ca. 17-15 ka BP) and

following (>13 ka BP) the ACR (Figure 2d) is consistent with a drier climate under a weaker southern westerly flow. These trends in proxy-inferred hydroclimate across Tasmania indicate either a strengthening of the westerly flow at their northern edge or a northward displacement of the westerlies during the ACR. The modern zone of maximum westerly winds speed lies between 50-60°S (Garreaud et al., 2009). A reduction in westerly wind-driven upwelling at marine core site TN057-13PC (located at 53.2°S, 5.1°E; Figure1a) on the southern edge of the southern westerlies during the ACR (Anderson et al., 2009) (Figure 3g) is synchronous with our inference of an increase in westerly flow at their northern edge in Tasmania (see Supplementary Information Table S1). This synchronicity of the ACR signal across the Southern Hemisphere suggests that a northward shift in the Australian sector is more likely than a stationary strengthening.

Our composite pollen data (see Figs. S4-5) from across western Tasmania indicate a regional expansion of Poaceae pollen (indicative of grassland; Figure 2f) during the ACR at the expense of *Phyllocladus aspleniifolius* (Figure 2e), a lowland temperate rainforest tree. Forests replaced grasslands during the last deglaciation in Tasmania in response to increasing temperature (Colhoun, 2000; Fletcher and Thomas, 2010), and our pollen data reflect a short-lived reversal of this trend in response to a temperature decrease during the ACR. Cooling over Tasmania is supported by proxy and model-based reconstructions of the ACR across the mid- to high-latitudes of the Southern Hemisphere (Koffman et al., 2017; Pedro et al., 2016; Putnam et al., 2010; Vandergoes et al., 2008). Collectively, our data indicate reduced temperature and increased southern westerly flow over Tasmania during the ACR that resulted in a cool and wet climate on the mountainous west coast sites, and a cool and dry climate on the lowland east coast sites.

We observe a synchronous and in-phase relationship between southern westerly changes over Tasmania and changes in the strength of the Leeuwin Current (De Deckker et al., 2012) (inferred from

core MD03-2611 in the Great Australian Bight; Figure1a), a surface ocean current that delivers warm tropical water from the Indo-Pacific Warm Pool to southern Australia (carrying tropical foraminifera such as *Globigerinoides ruber*) (Figure 3d) (Weaver and Middleton, 1989). The Leeuwin current is strongest in the Austral winter, when the northerly displaced southern westerlies accelerate the current along Australia's southern coast (Cirano and Middleton, 2004). We suggest the increased proportion of tropical foraminifera observed in MD03-2611 during the ACR can be explained by a northward-shifted southern westerly wind flow over the Australian sector. This shift would strengthen the Leeuwin Current along the south coast of Australia, in a similar way as seasonal migrations of the southern westerlies do today (Figure 3d).

Northward migration of the southern westerlies during the ACR is consistent, from an atmospheric dynamics perspective, with the documented northward shift of the ITCZ over northern Australia (Ayliffe et al., 2013; Ceppi et al., 2013; Denniston et al., 2013). The tendency for the ITCZ and southern westerlies to shift in the same direction is explained in detail elsewhere (Ceppi et al., 2013; Lee et al., 2011) and is documented by empirical data in the Australian sector during the Holocene (Mariani et al., 2018). In brief, a northward shift of the ITCZ is associated with strengthening of the Southern Hemisphere Hadley circulation delivering increased heat and eddy-momentum flux into the Southern Hemisphere subtropics. The increased momentum flux strengthens the subtropical jet and pulls the eddy driven jet (of which the surface expression is the southern westerlies) northward (Ayliffe et al., 2013; Denniston et al., 2013; Ceppi et al., 2013; Chiang et al., 2014) (Figure 6).

Importantly, our interpretation reconciles southern westerly proxy data spanning the ACR in the Australian region (De Deckker et al., 2012) with southern westerly behaviour elsewhere in the Southern Hemisphere. Rainforest declines in northeastern Brazil and the expansion of Magellanic moorland in western Patagonia indicate a northward shift in both the ITCZ and southern westerlies

between 15-13 ka BP (Montade et al., 2015). Recent Antarctic ice core based evidence show zonal shifts in moisture sources that similarly indicate northward movement of the westerlies during the ACR as well as earlier abrupt glacial climate changes (Buizert et al., 2018; Markle et al., 2017).

Our results provide further empirical evidence for the dynamics-based view that millennial scale climate variability involves major global reorganisation of ocean and atmospheric circulation and heat transport (Buizert et al., 2018; Markle et al., 2017; Pedro et al., 2016). The much-cited thermal ocean seesaw mechanism (Stocker and Johnson, 2003) is only one component of this larger coupled ocean-atmosphere reorganisation. Enhanced northward ocean heat transport is the primary energy source sustaining the Northern Hemisphere warming of the Bølling-Allerød and the South Atlantic and Southern Ocean cooling of the ACR (Pedro et al., 2018). The northern warming is abrupt (decadal scale) because it is associated with breakdown of stratification, release of accumulated sub-surface heat and rapid sea ice retreat in the North Atlantic and Nordic seas (Dokken et al., 2016; Sadatzki et al., 2018, Capron et al., 2021). The large-scale atmospheric counterpart to these changes stems from the effective northward shift of the thermal equator, which sets the position of the Hadley circulation and ITCZ. In shifting north, the cross equatorial Hadley cell gathers more energy from the warmer (northern) hemisphere for redistribution to the cooler (southern) hemisphere (Hartman et al., 2016), i.e. the dynamic atmospheric response acts to reduce the thermal imbalance between the hemispheres (see e.g. Fig 4 of Pedro et al. 2018). As detailed by Ceppi et al., (2013), and noted earlier, the northward shift of the westerlies occurs because a stronger cross-equatorial Hadley circulation also fluxes more momentum into the southern hemisphere subtropics, causing northward intensification of the eddy-driven jet and its surface expression in the southern westerlies.

An alternative hypothesis to the above ‘extended thermal seesaw’ was recently proposed by Denton et al, (2021). In their ‘Zealandia Switch’, orbitally-forced changes in southern hemisphere insolation drive millennial-scale variability in the position of the southern westerlies. When combined with the physical constraints of the Australian/Zealandia bathymetric footprint, these wind changes are

proposed to affect the global heat budget through the regulation of heat transport from the Tropical Pacific into the northern and southern hemisphere. We cannot exclude that this mechanism contributes to SH cooling during the ACR. However, the extended thermal seesaw framework has the advantages of satisfying the north-south timing, amplitude and spatial pattern of observed for millennial scale climate variations in multiple data compilations and data—model comparisons [e.g. Menviel et al., 2011; Pedro et al., 2016; Buizert et al., 2018, Corrick et al., 2020; Anderson et al., 2021, Capron et al., 2021]. Whether the 'Zealandia Switch' hypothesis satisfies such tests remains to be elucidated.

The northward shift of the southern westerlies during the ACR is synchronous with a reduction in Southern Ocean upwelling inferred from opal burial rates at TN057-13-4PC situated at 53°S, 5°E and with a CO_2 plateau in Antarctic ice cores (Figure 3i). Similarly, our evidence for southward shifted westerlies during the periods of deglacial warming that bracket the ACR aligns with increases in inferred Southern Ocean upwelling and intervals of CO_2 rise (Figure 3g,h). These results are consistent with the hypothesis that the position of the southern westerlies contributed to the observed deglacial CO_2 trends (Anderson et al., 2009; Toggweiler et al., 2006, Rae et al., 2018, Allen et al., 2019): i.e. enhanced Southern Ocean upwelling contributing to CO_2 outgassing when the winds were shifted southward toward Drake Passage and reduced outgassing when the winds shifted back northward, intensifying over Tasmania, during the ACR.

Acknowledgements

MSF was funded by Australian Research Council grants (DI110100019, IN140100050, IN170100062, IN170100063). JBP received support from the Australian Government as part of the Antarctic Science Collaboration Initiative program. We thank two anonymous reviewers for their positive and constructive reviews of an initial draft of this manuscript.

References

Anderson, R.F., Ali, S., Bratmiller, L.I., Nielsen, S.H.H., Fleisher, M.Q., Anderson, B.E., Burkle, L.H., 2009. Wind-Driven Upwelling in the Southern Ocean and the Deglacial Rise in Atmospheric CO_2. Science 323, 1443-1448.

Allen, K.A., Sikes, E.L., Anderson, R.F., Rosenthal, Y., 2020. Rapid Loss of CO2 From the South Pacific Ocean During the Last Glacial Termination. Paleoceanography and Paleoclimatology 35, e2019PA003766.

Anderson H.J., J.B. Pedro, H.C. Bostock, Z. Chase, T.L. Noble, 2021. Southern Ocean Sea Surface Temperature Response to Millennial-Scale Climate Change During Marine Isotope Stage 3: A Compilation. Quaternary Science Reviews 255, 106821, https://doi.org/10.1016/j.quascirev.2021.106821.

Ayliffe, L.K., Gagan, M.K., Zhao, J.-x., Drysdale, R.N., Hellstrom, J.C., Hantoro, W.S., Griffiths, M.L., Scott-Gagan, H., St Pierre, E., Cowley, J.A., 2013. Rapid interhemispheric climate links via the Australasian monsoon during the last deglaciation. Nature Communications 4.

Blaauw, M., Christen, J.A., 2011. Flexible paleoclimate age-depth models using an autoregressive gamma process. Bayesian Analysis 6, 457-474.

Blarquez, O., Vannière, B., Marlon, J.R., Daniau, A.-L., Power, M.J., Brewer, S., Bartlein, P.J., 2014. paleofire: an R package to analyse sedimentary charcoal records from the Global Charcoal Database to reconstruct past biomass burning. Computers & Geosciences 72, 255-261.

Bowman, D.M.J.S., Brown, M.J., 1986. Bushfires in Tasmania: a botanical approach to anthropological questions. Archaeology in Oceania 21, 166-171.

Box, G.E., Cox, D.R., 1964. An analysis of transformations. Journal of the Royal Statistical Society: Series B (Methodological) 26, 211-243.

Buizert, C., Sigl, M., Severi, M., Markle, B.R., Wettstein, J.J., McConnell, J.R., Pedro, J.B., Sodemann, H., Goto-Azuma, K., Kawamura, K., 2018. Abrupt ice-age shifts in southern westerly winds and Antarctic climate forced from the north. Nature 563, 681.

Capron, E., S.O. Rasmussen, T. J. Popp, T. Erhardt, H. Fischer, A. Landais, J.B. Pedro, G. Vettoretti, A. Grinsted, V. Gkinis, B. Vaughn, A. Svensson, B. M. Vinther, J. W. C. White. 2021. Multiple expressions in the anatomy of past abrupt warmings recorded in Greenland ice, Nature Communications 12:2106, 2021, https://doi.org/10.1038/s41467-021-22241-w.

Ceppi, P., Hwang, Y.T., Liu, X., Frierson, D.M., Hartmann, D.L., 2013. The relationship between the ITCZ and the Southern Hemispheric eddy-driven jet. Journal of Geophysical Research: Atmospheres 118, 5136-5146.

Cirano, M., Middleton, J.F., 2004. Aspects of the mean wintertime circulation along Australia's southern shelves: Numerical studies. Journal of Physical Oceanography 34, 668-684.

Chiang, J.C.H., Lee, S.-Y., Putnam, A.E., Wang, X., 2014. South Pacific Split Jet, ITCZ shifts, and atmospheric North-South linkages during abrupt climate changes of the last glacial period. Earth and Planetary Science Letters 406, 233-246.

Cleveland, W.S., 1979. Robust locally weighted regression and smoothing scatterplots. Journal of the American statistical association 74, 829-836.

Cohen, A.S., 2003. Paleolimnology: the history and evolution of lake systems. Oxford University Press.

Colhoun, E.A., 2000. Vegetation and climate during the last interglacial–glacial cycle in western Tasmania, Australia. Palaeogeography, Palaeoclimatology, Palaeoecology 155, 195-209.

Corrick E.C., R.N. Drysdale, J.C. Hellstrom, E. Capron, S.O. Rasmussen, X. Zhang, D. Fleitmann, I. Couchoud, E. Wolff. 2020. Synchronous timing of abrupt climate changes during the last glacial period, Science 369, 963–969, 10.1126/science.aay5538.

Croudace, I.W., Rothwell, R.G., 2015. Micro-XRF Studies of Sediment Cores: Applications of a non-destructive tool for the environmental sciences. Springer.

Daniau, A.L., Bartlein, P.J., Harrison, S., Prentice, I.C., Brewer, S., Friedlingstein, P., Harrison-Prentice, T., Inoue, J., Izumi, K., Marlon, J., 2012. Predictability of biomass burning in response to climate changes. Global Biogeochemical Cycles 26.

De Deckker, P., Moros, M., Perner, K., Jansen, E., 2012. Influence of the tropics and southern westerlies on glacial interhemispheric asymmetry. Nature Geoscience 5, 266-269.

Denniston, R.F., Wyrwoll, K.-H., Polyak, V.J., Brown, J.R., Asmerom, Y., Wanamaker, A.D., LaPointe, Z., Ellerbroek, R., Barthelmes, M., Cleary, D., 2013. A Stalagmite record of Holocene Indonesian–Australian summer monsoon variability from the Australian tropics. Quaternary Science Reviews 78, 155-168.

Denton, G.H., Anderson, R.F., Toggweiler, J.R., Edwards, R.L., Schaefer, J.M., Putnam, A.E., 2010. The Last Glacial Termination. Science 328, 1652.

Denton, G.H., Putnam, A.E., Russell, J.L., Barrell, D.J., Schaefer, J.M., Kaplan, M.R., Strand, P.D., 2021. The Zealandia Switch: Ice age climate shifts viewed from Southern Hemisphere moraines. Quaternary Science Reviews 257, 106771.

Eugster, H.P., Hardie, L.A., 1978. Saline lakes, lakes. Springer, pp. 237-293.

Faegri, K., Iversen, J., 1989. Textbook of pollen analysis. Wiley, New York.

Fletcher, M.-S., Moreno, P.I., 2012. Have the Southern Westerlies changed in a zonally symmetric manner over the last 14,000 years? A hemisphere-wide take on a controversial problem. Quaternary International 253, 32–46.

Fletcher, M.-S., Thomas, I., 2007. Modern pollen–vegetation relationships in western Tasmania, Australia. Review of Palaeobotany and Palynology 146, 146-168.

Fletcher, M.-S., Thomas, I., 2010. A quantitative Late Quaternary temperature reconstruction from western Tasmania, Australia. Quaternary Science Reviews 29, 2351-2361.

Fletcher, M.-S., Wolfe, B.B., Whitlock, C., Pompeani, D.P., Heijnis, H., Haberle, S.G., Gadd, P.S., Bowman, D.M.J.S., 2014. The legacy of mid-Holocene fire on a Tasmanian montane landscape. Journal of Biogeography 41, 476-488.

Garreaud, R.D., 2007. Precipitation and circulation covariability in the extratropics. Journal of Climate 20, 4789-4797.

Garreaud, R.D., Vuille, M., Compagnucci, R., Marengo, J., 2009. Present-day South American climate. Palaeogeography Palaeoclimatology Palaeoecology 281, 180-195.

Gillett, N.P., Kell, T.D., Jones, P.D., 2006. Regional climate impacts of the Southern Annular Mode. Geophysical Research Letters 33, L23704.

Haberzettl, T., Corbella, H., Fey, M., Janssen, S., Lucke, A., Mayr, C., Ohlendorf, C., Schabitz, F., Schleser, G.H., Wille, M., 2007. Lateglacial and Holocene wet--dry cycles in southern Patagonia: chronology, sedimentology and geochemistry of a lacustrine record from Laguna Potrok Aike, Argentina. The Holocene 17, 297.

Hartmann, D., 2016. Global Physical Climatology, Second Edition. Elsevier, Amsterdam, Netherlands, 485pp.

Hogg, A.G., Heaton, T.J., Hua, Q., Palmer, J.G., Turney, C.S., Southon, J., Bayliss, A., Blackwell, P.G., Boswijk, G., Ramsey, C.B., 2020. SHCal20 Southern Hemisphere calibration, 0–55,000 years cal BP. Radiocarbon, 1-20.

Kelts, K., Hsü, K., 1978. Freshwater carbonate sedimentation, Lakes. Springer, pp. 295-323.

Koffman, T.N., Schaefer, J.M., Putnam, A.E., Denton, G.H., Barrell, D.J., Rowan, A.V., Finkel, R.C., Rood, D.H., Schwartz, R., Plummer, M.A., 2017. A beryllium-10 chronology of late-glacial moraines in the upper Rakaia valley, Southern Alps, New Zealand supports Southern-Hemisphere warming during the Younger Dryas. Quaternary Science Reviews 170, 14-25.

Kunsch, H.R., 1989. The jackknife and the bootstrap for general stationary observations. The annals of Statistics, 1217-1241.

Kylander, M.E., Ampel, L., Wohlfarth, B., Veres, D., 2011. High-resolution X-ray fluorescence core scanning analysis of Les Echets (France) sedimentary sequence: new insights from chemical proxies. Journal of Quaternary Science 26, 109-117.

Lee, S.Y., Chiang, J.C., Matsumoto, K., Tokos, K.S., 2011. Southern Ocean wind response to North Atlantic cooling and the rise in atmospheric CO2: Modeling perspective and paleoceanographic implications. Paleoceanography 26.

Mariani, M., Fletcher, M.-S., 2017. Long-term climate dynamics in the extra-tropics of the South Pacific revealed from sedimentary charcoal analysis. Quaternary Science Reviews 173, 181-192.

Mariani, M., Fletcher, M.-S., Drysdale, R.N., Saunders, K.M., Heijnis, H., Jacobsen, G., Zawadzki, A., 2018. Coupling of the Intertropical Convergence Zone and Southern Hemisphere mid-latitude climate during the early to mid-Holocene. Geology.

Mariani, M., Fletcher, M.S., 2016. The Southern Annular Mode determines inter-annual and centennial-scale fire activity in temperate southwest Tasmania, Australia. Geophysical Research Letters 43.

Markle, B.R., Steig, E.J., Buizert, C., Schoenemann, S.W., Bitz, C.M., Fudge, T., Pedro, J.B., Ding, Q., Jones, T.R., White, J.W., 2017. Global atmospheric teleconnections during Dansgaard-Oeschger events. Nature Geoscience 10, 36-40.

Marlon, J.R., Bartlein, P.J., Carcaillet, C., Gavin, D.G., Harrison, S.P., Higuera, P.E., Joos, F., Power, M., Prentice, I., 2008. Climate and human influences on global biomass burning over the past two millennia. Nature Geoscience 1, 697-702.

McManus, J.F., Francois, R., Gherardi, J.M., Keigwin, L.D., Brown-Leger, S., 2004. Collapse and rapid resumption of Atlantic meridional circulation linked to deglacial climate changes. Nature 428, 834.

McWethy, D., Higuera, P., Whitlock, C., Veblen, T., Bowman, D., Cary, G., Haberle, S., Keane, R., Maxwell, B., McGlone, M., 2013. A conceptual framework for predicting temperate ecosystem sensitivity to human impacts on fire regimes. Global Ecology and Biogeography 22, 900-912.

Menviel, L., Timmermann, A., Elison Timm, O., Mouchet A., 2011. Deconstructing the Last Glacial termination: the role of millennial and orbital-scale forcings, Quaternary Science Reviews, 30, 1155-1172, doi:10.1016/j.quascirev.2011.02.005.

Montade, V., Kageyama, M., Combourieu-Nebout, N., Ledru, M.-P., Michel, E., Siani, G., Kissel, C., 2015. Teleconnection between the Intertropical Convergence Zone and southern westerly winds throughout the last deglaciation. Geology 43, 735-738.

Pedro, J.B., Bostock, H.C., Bitz, C.M., He, F., Vandergoes, M.J., Steig, E.J., Chase, B.M., Krause, C.E., Rasmussen, S.O., Markle, B.R., 2016. The spatial extent and dynamics of the Antarctic Cold Reversal. Nature Geoscience 9, 51-55.

Putnam, A.E., Denton, G.H., Schaefer, J.M., Barrell, D.J., Andersen, B.G., Finkel, R.C., Schwartz, R., Doughty, A.M., Kaplan, M.R., Schlüchter, C., 2010. Glacier advance in southern middle-latitudes during the Antarctic Cold Reversal. Nature Geoscience 3, 700-704.

Rae, J.W.B., Burke, A., Robinson, L.F. et al. CO2 storage and release in the deep Southern Ocean on millennial to centennial timescales. Nature 562, 569–573 (2018). https://doi.org/10.1038/s41586-018-0614-0

Sadatzki, H., et al., 2019. Sea ice variability in the southern Norwegian Sea during glacial Dansgaard-Oeschger climate cycles. Sci. Adv. 5, eaau6174, doi: 10.1126/sciadv.aau6174.

Siani, G., Michel, E., De Pol-Holz, R., DeVries, T., Lamy, F., Carel, M., Isguder, G., Dewilde, F., Lourantou, A., 2013. Carbon isotope records reveal precise timing of enhanced Southern Ocean upwelling during the last deglaciation. Nature Communications 4, 2758.

Sigman, D.M., Fripiat, F., Studer, A.S., Kemeny, P.C., Martínez-García, A., Hain, M.P., Ai, X., Wang, X., Ren, H., Haug, G.H., 2020. The Southern Ocean during the ice ages: A review of the Antarctic surface isolation hypothesis, with comparison to the North Pacific. Quaternary Science Reviews, 106732.

Styger, J., Kirkpatrick, J.B., 2015. Less than 50 millimetres of rainfall in the previous month predicts fire in Tasmanian rainforest. Papers and Proceedings of the Royal Society of Tasmania 149, 1-5.

Toggweiler, J.R., Russell, J.L., Carson, S.R., 2006. Midlatitude westerlies, atmospheric CO2, and climate change during the ice ages. Paleoceanography 21, PA2005.

Vandergoes, M.J., Dieffenbacher-Krall, A.C., Newnham, R.M., Denton, G.H., Blaauw, M., 2008. Cooling and changing seasonality in the Southern Alps, New Zealand during the Antarctic Cold Reversal. Quaternary Science Reviews 27, 589-601.

Weaver, A.J., Middleton, J.H., 1989. On the dynamics of the Leeuwin Current. Journal of Physical Oceanography 19, 626-648.

408

409

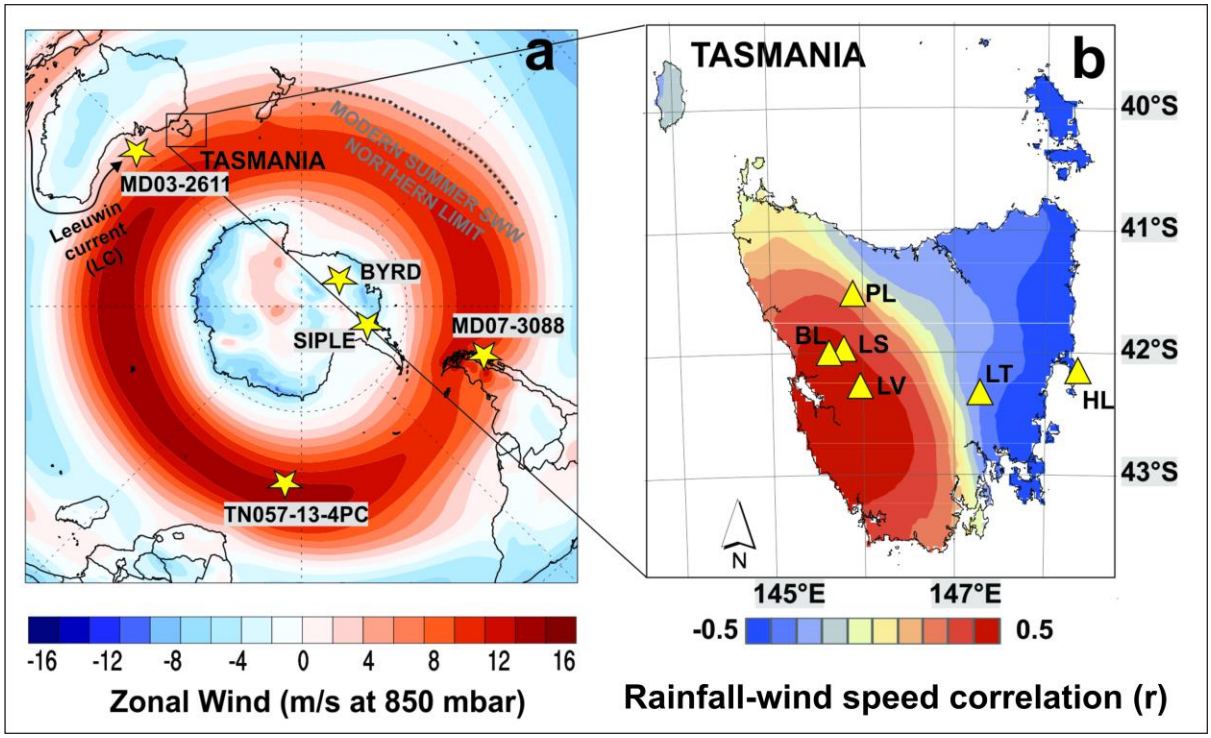

410

411 **Figure 1 (a) A map of zonal (southern westerly) wind speed showing the location of proxy sites**
412 **mentioned in the text and (b) a correlation map of southern westerly wind speed and rainfall in**
413 **Tasmania with sites analysed in this study: LV – Lake Vera; BL – Basin Lake; LS – Lake Selina; PL –**
414 **Paddy's Lake; LT – Lake Tiberias and HL – Hazards Lagoon.**

415

416

417

418

419

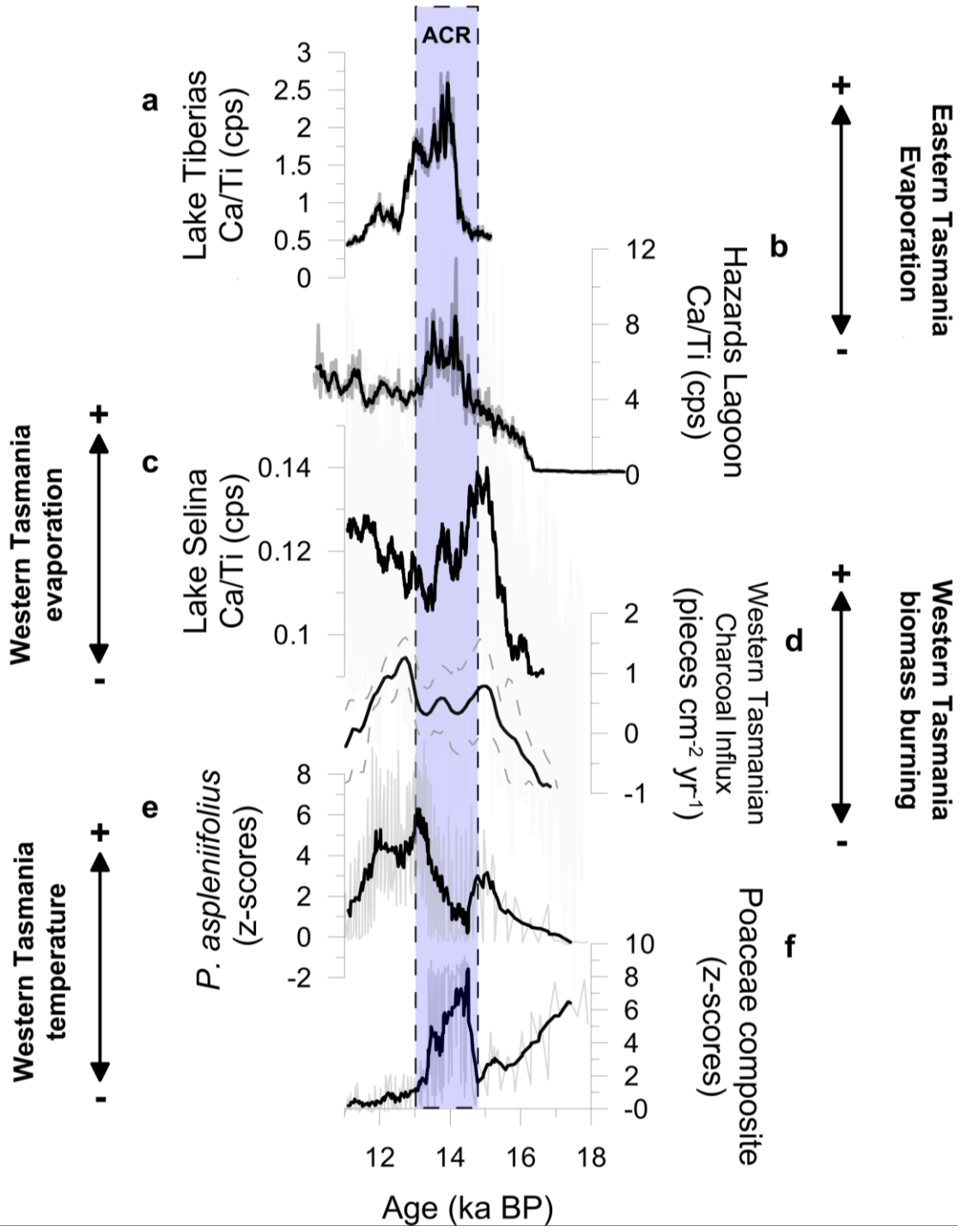

420

421 **Figure 2 Proxy data spanning the period between 18-11 ka BP showing (a) Lake Tiberias and (b)**
422 **Hazards Lagoon and (c) Lake Selina Ca/Ti ratio, indicating changes in evaporite deposition. Black**
423 **curves indicate the weighted average (5-year window) for (a), (b) and weighted average (43-year**
424 **window) for (c); (d) western Tasmania charcoal influx composite (n=3) showing upper and lower**
425 **confidence intervals (dashed grey lines) indicating moisture-driven changes in fire activity; (e)**

composite pollen (n=6) of the hygrophilous rainforest tree *Phyllocladus aspleniifolius*; and (f) composite Poaceae pollen curve (n=6) indicating changes in the grassland component of western Tasmanian pollen records. Black curves for both (e) and (f) indicate the weighted average (7-year window). Chronologies and associated uncertainties for all records used to create composite curves are presented in Supplementary Table 1 and Supplementary Figure 3.

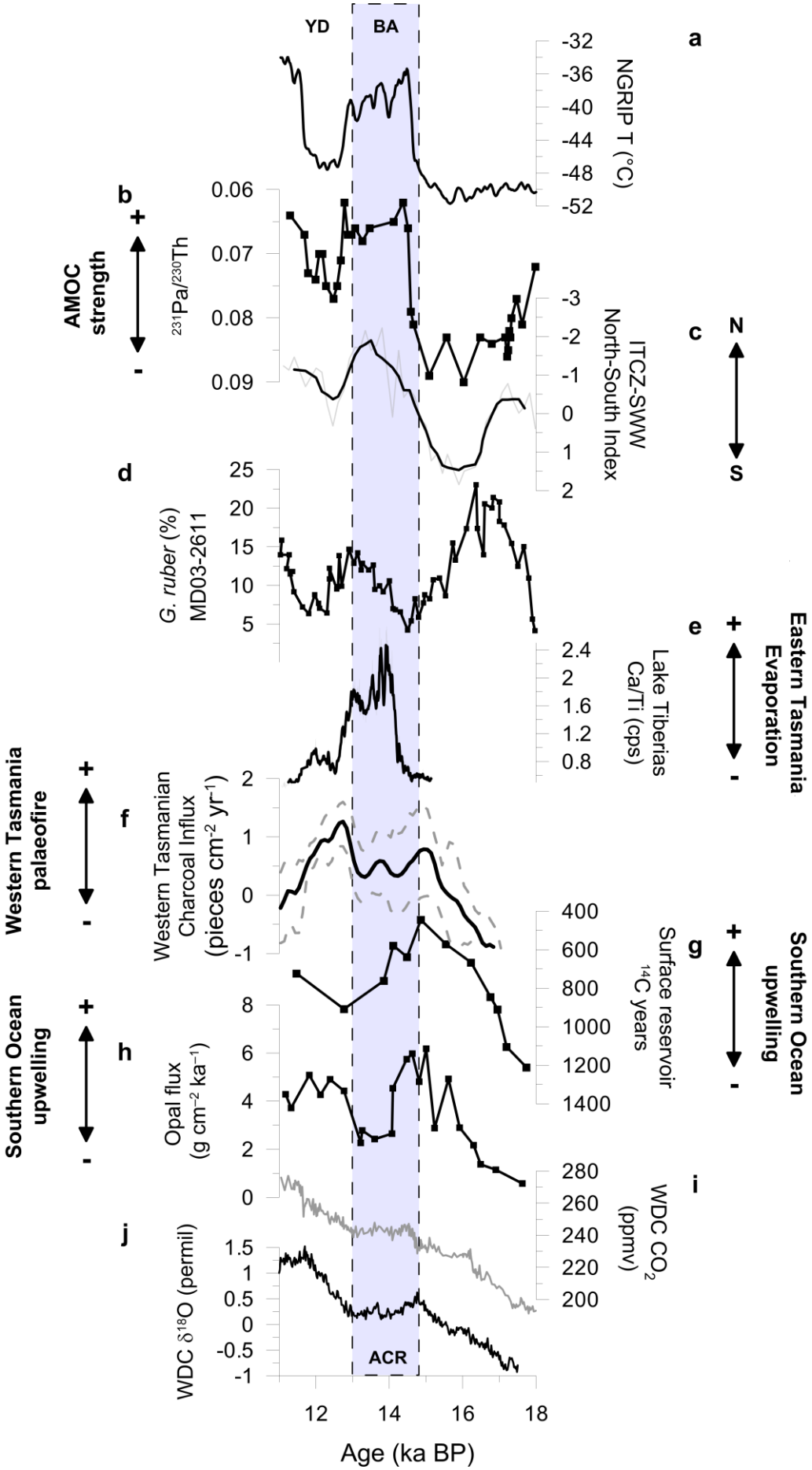
YD
BA
ACR
a
NGRIP T (°C)
-32
-36
-40
-44
-48
-52
b
AMOC strength
+
-
^{231}Pa/^{230}Th
0.06
0.07
0.08
0.09
c
N
S
ITCZ-SWW North-South Index
-3
-2
-1
0
1
2
d
G. ruber (%) MD03-2611
25
20
15
10
5
e
Eastern Tasmania Evaporation
Lake Tiberias Ca/Ti (cps)
2.4
2
1.6
1.2
0.8
f
Western Tasmania palaeofire
Western Tasmanian Charcoal Influx (pieces cm^{-2} yr^{-1})
2
1
0
-1
g
Southern Ocean upwelling
Surface reservoir ^{14}C years
400
600
800
1000
1200
1400
h
Southern Ocean upwelling
Opal flux (g cm^{-2} ka^{-1})
8
6
4
2
0
i
WDC CO_2 (ppmv)
280
260
240
220
200
j
WDC δ^{18}O (permil)
1.5
1
0.5
0
-0.5
-1
12
14
16
18
Age (ka BP)

Figure 3 Global proxy data spanning the period between 18-11 ka showing (a) Proxy NGRIP surface-air temperature (^{15}N and diffusion-based reconstruction) (Buizert et al., 2018); (b) Proxy AMOC strength ($^{231}Pa/^{230}Th$) from the Bermuda Rise (McManus et al., 2004); (c) Normalized index summarizing common latitudinal shifts of both the ITCZ and the southern westerlies (Montade et al., 2015); (d) *Globigerinoides ruber* % from ocean core MD03-2611 at 37°S (De Deckker et al., 2012) a tropical foraminifera indicating changes in the strength of the Leeuwin Current; (e) Lake Tiberias Ca/Ti ratio showing changes in evaporation (this study); (f) western Tasmania charcoal influx composite (n=3) indicating moisture-driven changes in fire activity (this study); (g) radiocarbon surface reservoir age determined off the coast of Chile at 46°S (Siani et al., 2013) showing changes in wind-driven upwelling (De Deckker et al., 2012); (h) Southern Ocean Opal flux, a proxy for upwelling south of the Antarctic polar front from core TN057-13-4PC at 53°S showing changes in wind-driven upwelling (Anderson et al., 2009); and West Antarctic Ice Sheet Divide ice core (WDC) (i) CO_2 and (j) $\delta^{18}O$ (Buizert et al., 2018).

Funding:

Australian Research Council grant DI110100019

Australian Research Council grant IN140100050

Australian Research Council grant IN170100062

Australian Research Council grant IN170100063

Author contributions:

Conceptualization: MSF

Methodology: MSF, MM, JAA, KB, PSG, HH

Investigation: MSF, MM, JAA, KB

Visualization: MSF, MM, KB, TH

Funding acquisition: MSF, ALP

Project administration: MSF

Supervision: MSF

Writing – original draft: MSF, JP

Writing – review & editing: MSF, JP, TH, MM, JA, KB, MB, DAH, HH, PSG, ALP

Data and materials availability:

All data will be made available upon request

Figure 1

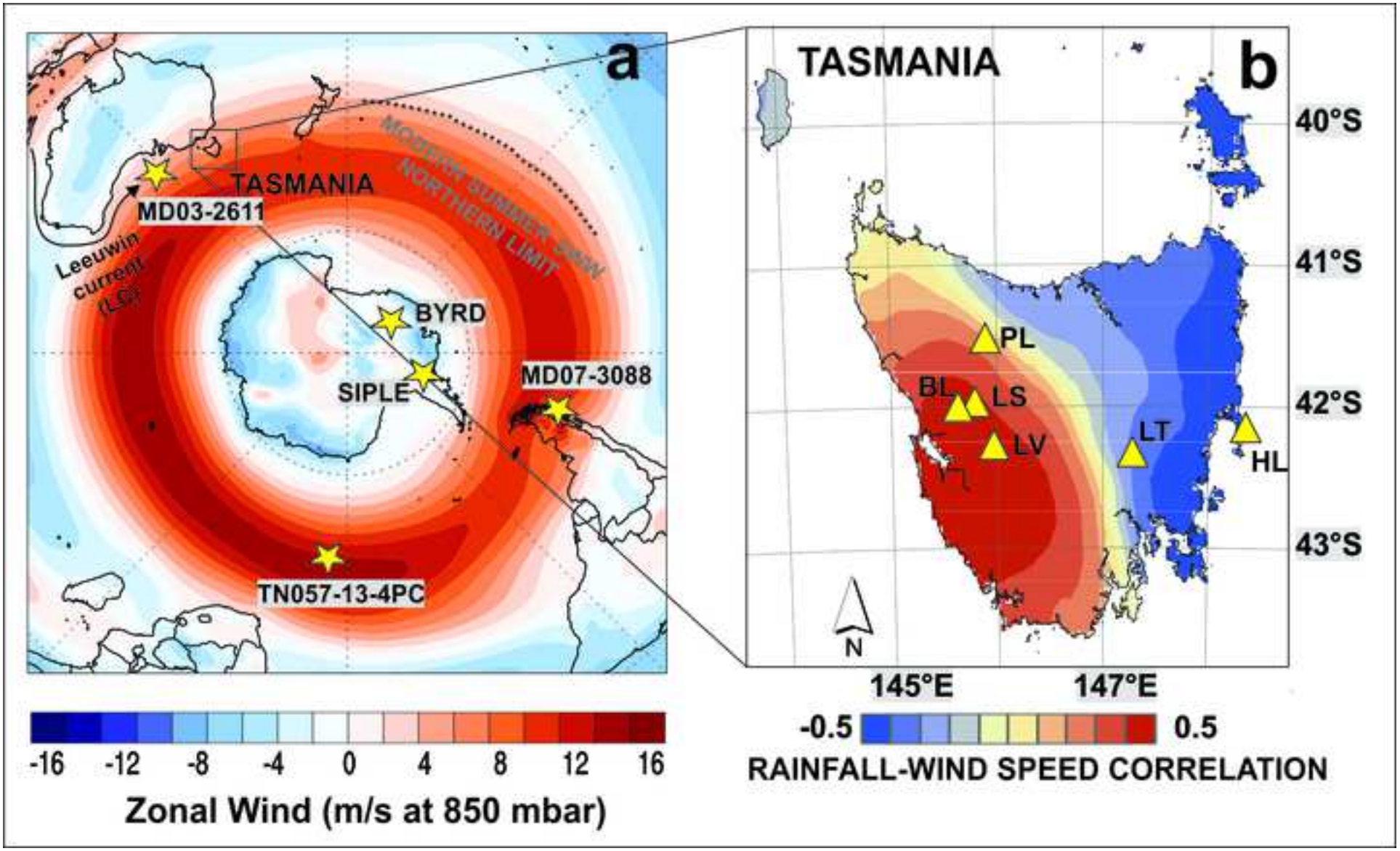

Figure 2

Click here to access/download;Figure;ACR TASMANIA.png

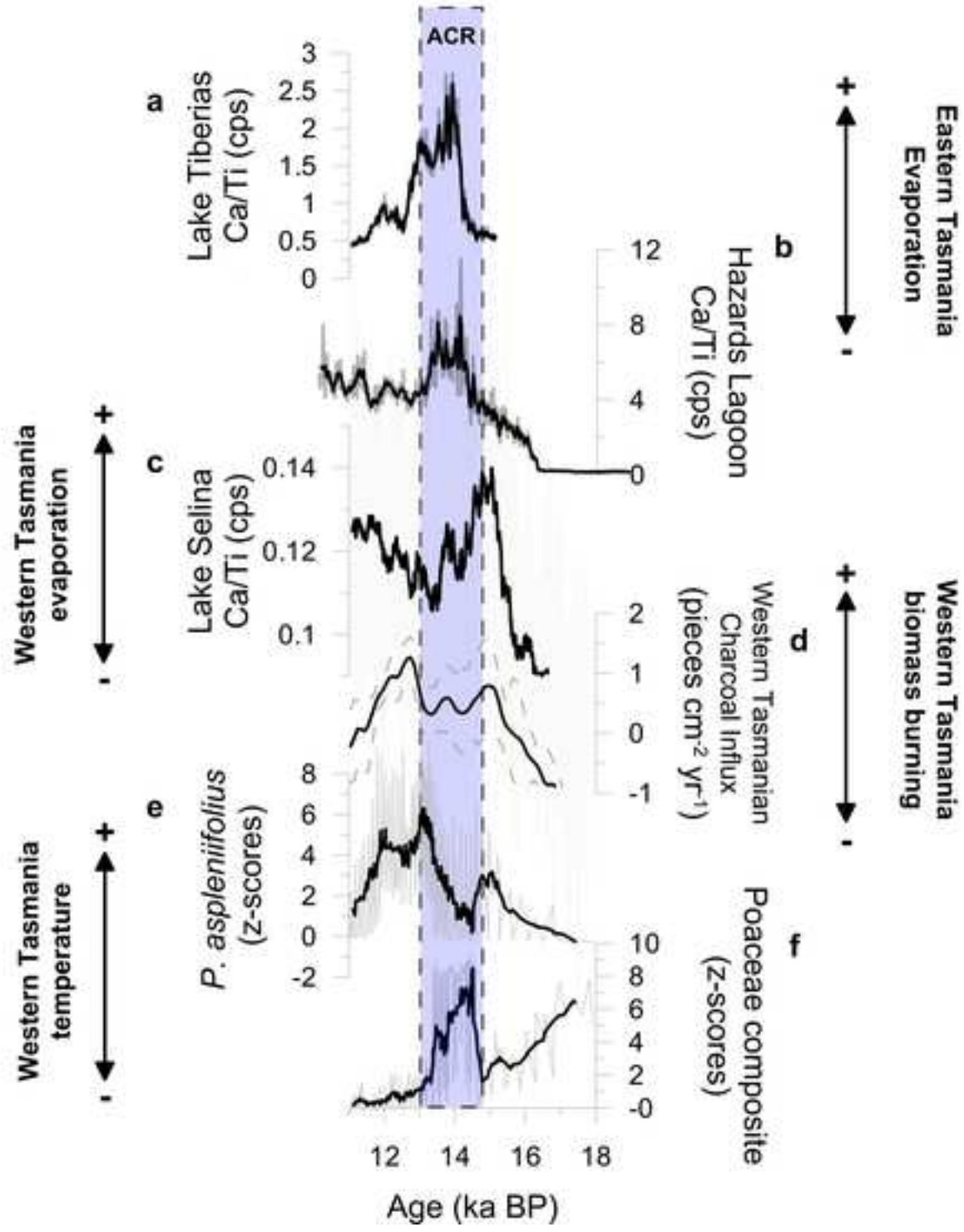

Figure 3

Click here to access/download;Figure;ACR REGIONAL_fixed.png

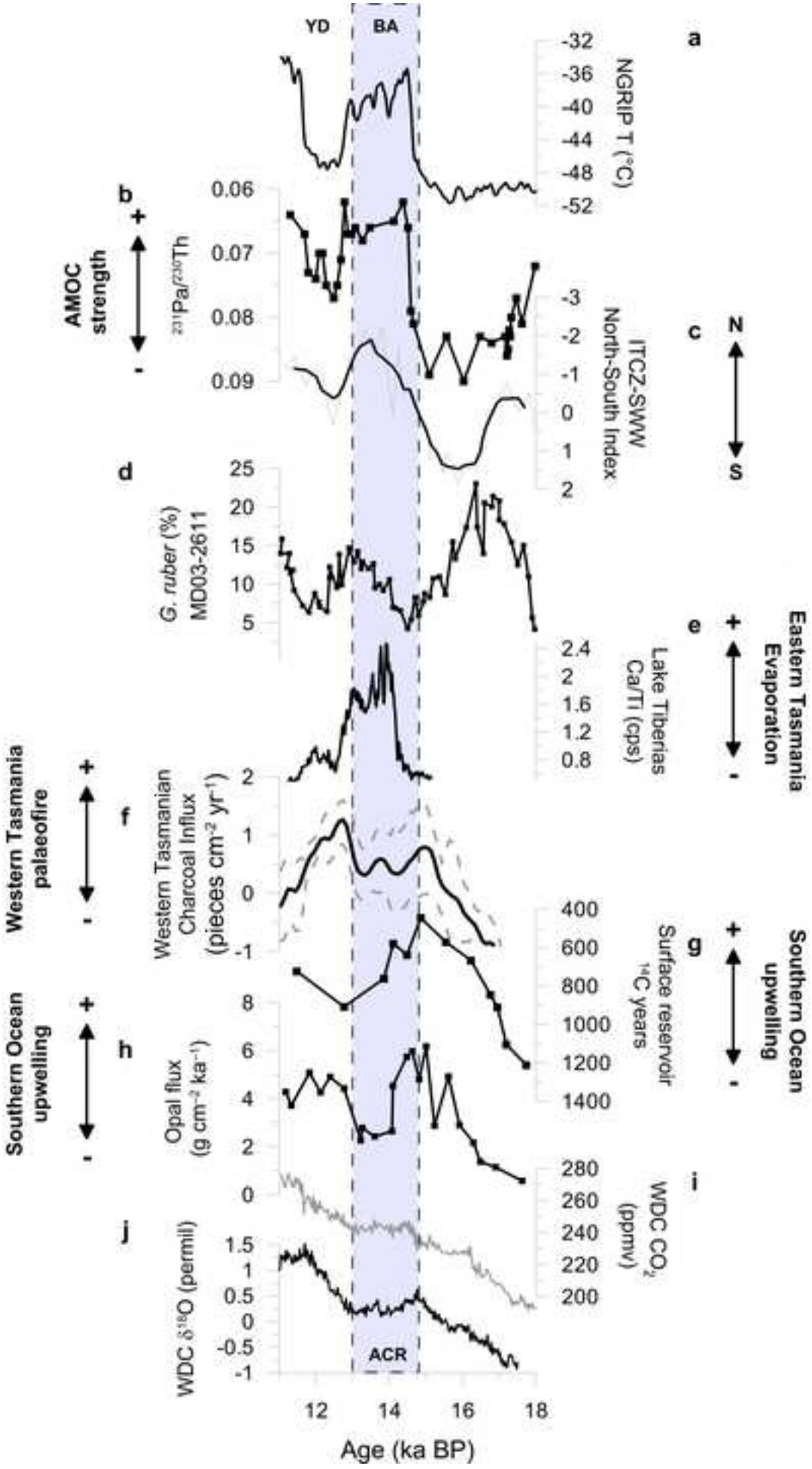

Declaration of interests

☒ The authors declare that they have no known competing financial interests or personal relationships that could have appeared to influence the work reported in this paper.

☐The authors declare the following financial interests/personal relationships which may be considered as potential competing interests:

Author contributions:

Conceptualization: MSF

Methodology: MSF, MM, JAA, KB, PSG, HH

Investigation: MSF, MM, JAA, KB

Visualization: MSF, MM, KB, TH

Funding acquisition: MSF, ALP

Project administration: MSF

Supervision: MSF